Proceedings of the 4th International Conference on Functional Materials and Civil Engineering
DOI: 10.54254/2755-2721/2026.38264

A Comparative Aerodynamic Performance Analysis of Fixed-Wing UAVs NACA0015 and NACA2415

Fanhe Kong

International Education College, Shenyang Aerospace University, Shenyang, China
hankkong0927@gmail.com

Abstract. Airfoil camber is a critical geometric parameter affecting aerodynamic characteristics, which directly determines the aerodynamic performance of aircraft. In recent years, unmanned aerial vehicles have been widely applied in various fields, and cargo Unmanned Aerial Vehicles (UAVs) are expected to become mainstream equipment for freight transportation. NACA0015 and NACA2415 are two airfoils with great potential for cargo UAV design. In this work, NACA2415 and NACA0015 are chosen as research cases. The computational fluid dynamics (CFD) method based on Reynolds-Averaged Navier-Stokes (RANS) equations and the SST k-ω turbulence model is used to perform numerical simulations and aerodynamic comparisons within the angle-of-attack range of 0° to 24°. The simulation results demonstrate that the NACA2415 airfoil achieves a higher lift coefficient and superior stall resistance at low angles of attack. Compared with NACA0015, NACA2415 is more suitable for fixed-wing cargo UAVs. Furthermore, this study reveals that airfoils with larger camber can generate higher lift under low angle-of-attack conditions.

Keywords: CFD, airofoil, pressure, lift and drag force

1. Introduction

Drones today figure prominently in all areas of life; fixed - wing models,with a proven ability to carry large loads, are used extensively for transport purposes [1]. With regard to wings , analysis of the aerodynamics of individual airfoil profiles is central to the design of an aircraft .The NACA four - digit airfoil series has many useful features — it lends itself well to construction and to simulation studies ,the present configuration is well suited for the fast-paced current development of drone technology .Both NACA0015 and NACA2415 have the same maximal thickness at the 15%chord location and exactly the same internal structures .With regard to the percentage of maximum curvature—relative to chord length—and to the placement of such a maximum along the chord, the respective values are 0%and 2%,or 0% and 40%,respectively .Such pairs of parameters now provide a framework for evaluating the aerodynamics of the two airfoil forms .

Among the aerodynamic indicators — namely the pressure coefficient, the lift coefficient, and the lift - to - drag ratio — there are ones that reflect accurately the aerodynamic properties of airfoil profiles. If one studies the dependence of wing parameters on various angles of attack and relates this to the onset of stalling at too great an angle, then one may evaluate separately the merits of each

© 2026 The Authors. This is an open access article distributed under the terms of the Creative Commons Attribution License 4.0 (https://creativecommons.org/licenses/by/4.0/).

DOI: 10.54254/2755-2721/2026.38264

of the two airfoil forms for fixed - wing Unmanned Aerial Vehicles (UAVs) and decide upon their respective uses.

Numerous scholars have conducted extensive research in this field; for instance, Touhid Ahmed Orvi found that the optimal lift-to-drag ratio for the NACA0015 airfoil is achieved with an NACA0015 airfoil featuring a cavity located at 70% chord length (0.7c), indicating optimal aerodynamic performance at moderate angles of attack [2]. Robiul I. Rubel and his colleagues compared the aerodynamic characteristics of the NACA0015 and NACA4415 airfoils [3]. Medyawanti performed a computational fluid dynamics (CFD) analysis of the NACA2415 and NACA2412 airfoils [4]. Zhao and Yang investigated the lift generated by various airfoils at different angles of attack within a turbulent flow model [5]. Matyushenko and Garbaruk improved the SST k–ω model and noted that the enhanced SST k–ω model is applicable only to the flow region adjacent to the airfoil [6]. For improving the aerodynamic performance of fixed-wing UAVs, Panagiotou and Yakinthos provided guiding principles [7]. Panagiotopoulos, Sakellariou, and Hatziefremidis documented the complete design, manufacturing, and testing process of an electrically powered flying-wing UAV [8].

The present work uses the CFD method in a uniform computational setup to investigate—systematically—the lift coefficient, drag coefficient [9, 10], and lift-to-drag ratio of the NACA0015 and NACA2415 airfoil profiles at angles of attack from 0 up to 24°, as well as to construct contour plots for pressure and for velocity field patterns. Such results help identify aerodynamic disparities between the two airfoils and assess their possible utility in fixed-wing UAV configurations.

2. Numerical method

2.1. Airfoil geometric model and meshing

The subjects of this study are the NACA0015 and NACA2415 airfoil profiles; their geometric models are shown in Figure 1, with a chord length of 1 m. The computational domain employs a C-type CFD domain is shown in Figure 2, with the inlet located 7.5 m from the leading edge and the outlet located 15 m from the trailing edge.A velocity inlet boundary is applied at the inlet, where the free-stream velocity is specified as 35 m/s, yielding a Reynolds number close to 2.4×10^6. For the outlet boundary, a pressure outlet condition with zero gauge pressure is adopted, while the airfoil wall is assigned the no-slip boundary condition.

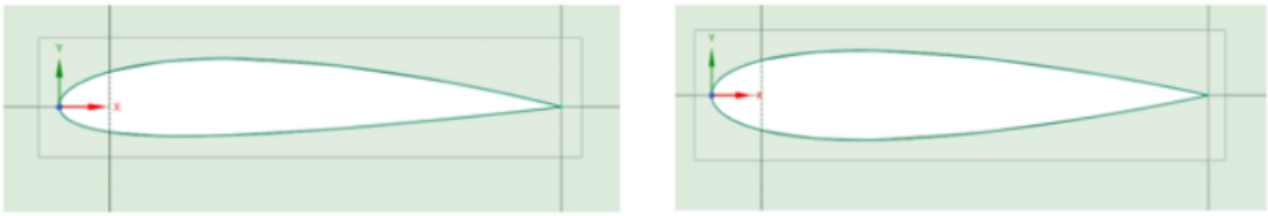

Figure 1. Geometric models of NACA0015 and NACA2415

DOI: 10.54254/2755-2721/2026.38264

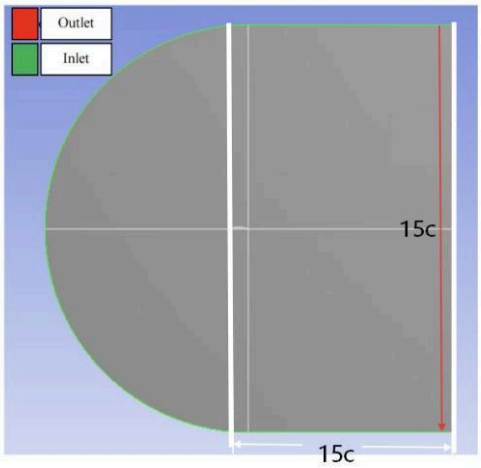

Figure 2. Computational domain of airfoil numerical simulation

2.2. Reynolds number and lift resistance calculation equation

This study requires the calculation of the aerodynamic characteristics of various airfoil profiles under low Reynolds number conditions; based on the Reynolds number equation, the Reynolds number is estimated to be approximately 2.4×10^6, and it is therefore decided to conduct the research under these conditions.

Reynolds number is as follows:

$$\mathrm{Re}=\frac{\rho \mathrm{VL}}{\mu} \tag{1}$$

Lift drag coefficient equation is as follows:

$$\mathrm{C_L}=2\mathrm{F_L}/\left(\rho \mathrm{V}^2\mathrm{A}\right),\mathrm{C_D}=2\mathrm{F_D}/\left(\rho \mathrm{V}^2 A\right) \tag{2}$$

2.3. Control equations and turbulence model

This paper employs the Reynolds-Averaged Navier–Stokes (RANS) equations, derived from the finite volume method, to solve problems involving incompressible viscous flows.

Navier–Stokes equations is as follows:

$$\frac{\partial \rho}{\partial \mathrm{t}}+\frac{\partial \rho \mathrm{u}}{\partial \mathrm{x}}+\frac{\partial \rho \mathrm{v}}{\partial \mathrm{y}}+\frac{\partial \rho \mathrm{w}}{\partial \mathrm{z}}=0 \tag{3}$$

The SST k-ω turbulence model is employed. This model utilizes a built-in mixing function-based partitioned solution approach to accurately simulate boundary layer flow near the wall surface while ensuring high computational stability in the far field. It is capable of precisely capturing both the attached flow over the airfoil across the entire attack angle range of 0°–24°, as well as the flow separation and progressive stall characteristics induced by the adverse pressure gradient at high

DOI: 10.54254/2755-2721/2026.38264

attack angles, thereby guaranteeing high accuracy in the calculation of lift, drag forces, and the lift-to-drag ratio.

2.4. Mesh generation and solution settings

The computational domain is discretized using a structured mesh; the wing profile's near-wake region is refined to ensure that the dimensionless wall distance y+ is less than 1, and thus satisfying the computational requirements for the direct numerical simulation of the viscous bottom layer under the SST·k-ω model; in the far-field region, the mesh is gradually coarsened to control the overall computational cost while maintaining accuracy. The total number of mesh cells is approximately 100,000; after verifying mesh independence, it was confirmed that the mesh meets the required computational accuracy criteria. The mesh generation diagrams for the NACA2425 and NACA0015 airfoils are shown in Figure 3.

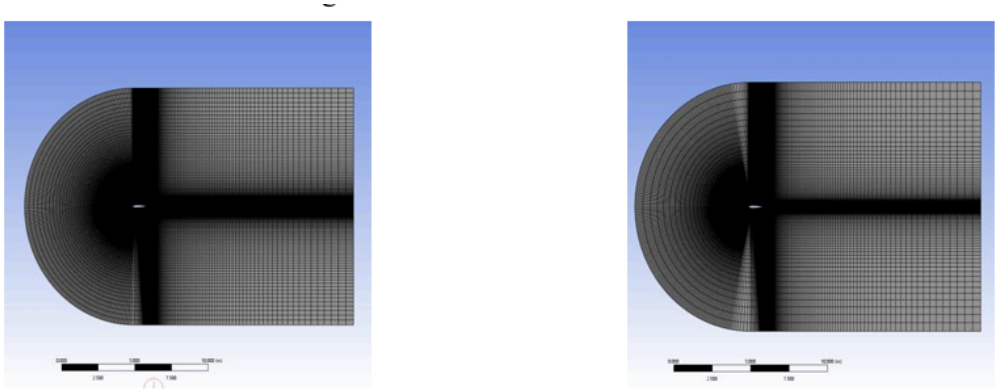

(a) NACA2415 mesh generation diagram (b) NACA0015 mesh generation diagram

Figure 3. Mesh generation diagrams for NACA2415 and NACA0015 profiles

The solver employs a pressure-based coupled solution algorithm; the momentum equation, the splash kinetic energy equation, and the specific dissipation rate equation are all discretized using second-order upwind schemes to enhance computational accuracy. The detailed solver configuration parameters are shown in Table 1.

Table 1. Solution parameter settings

import		
Free-stream velocity:	35	[m/s]
density:	1.225	[kg/m^3]
dynamic viscosity:	1.82e-5	[kg/ms]
Boundary layer length:	1.0	[m]
Expected Y+ value:	1.0	
output		
Reynolds number:	2.4e+6	
Expected wall distance:	1.1e-5	[m]

DOI: 10.54254/2755-2721/2026.38264

3. Results and discussion

3.1. Lift coefficient

Figure 4 compares the lift coefficients of the two airfoil profiles at various angles of attack; both the NACA0015 and NACA2415 profiles exhibit an increasing lift coefficient as the angle of attack rises within the range of 0°–16°. Due to its greater curvature, the NACA2415 profile generates a higher lift coefficient than the NACA0015 profile at the same angle of attack. At the same angle of attack, the curvature further induces stronger airflow deflection around the wing, enabling the NACA2415 profile to generate a larger circulation (Γ) compared to the symmetric NACA0015 profile, thereby producing greater lift. After entering the stall regime, the NACA0015 profile experiences a more rapid decline in lift and a more abrupt stall onset; in contrast, the NACA2415 profile's stall process is relatively smoother, demonstrating superior stall resistance characteristics.

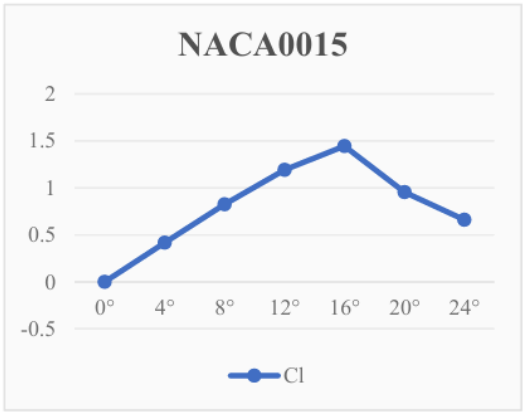

(a) NACA0015 lift coefficient variation curve diagram

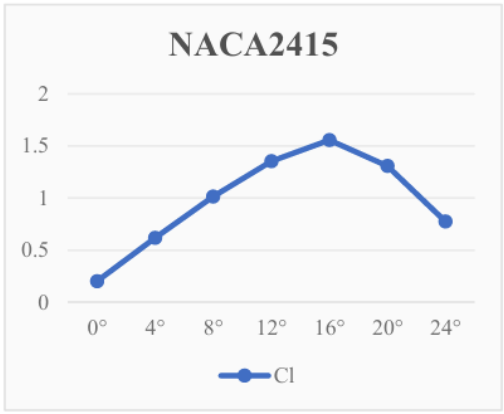

(b) NACA2515 lift coefficient variation curve diagram

Figure 4. Comparison of lift coefficients for NACA0015 and NACA2425 at different angles of attack

3.2. Coefficient of drag

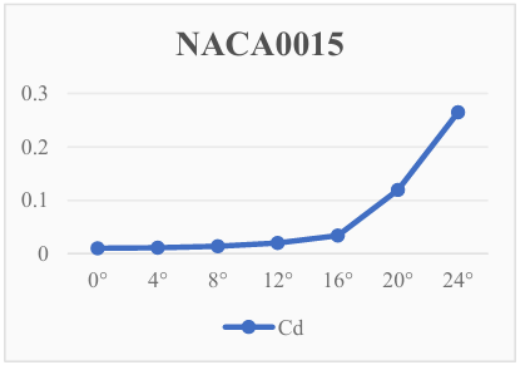

(a) NACA0015 drag coefficient variation curve

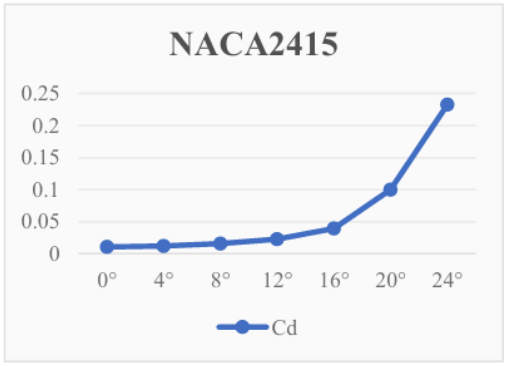

(b) NACA0015 drag coefficient variation curve

Figure 5. Comparison of lift coefficients for NACA0015 and NACA2415 at different angles of attack

DOI: 10.54254/2755-2721/2026.38264

As shown in Figure 5, the overall drag coefficients for both airfoil profiles are relatively low, and their increase is very gradual. The flow remains attached; the drag is primarily due to viscous friction drag on the airfoil surface, while the contribution of pressure difference drag is extremely small. Due to its inherent curvature, the NACA2415 airfoil exhibits a slightly higher drag coefficient at the same attack angle compared to the symmetric NACA0015 airfoil.

3.3. Pressure contour

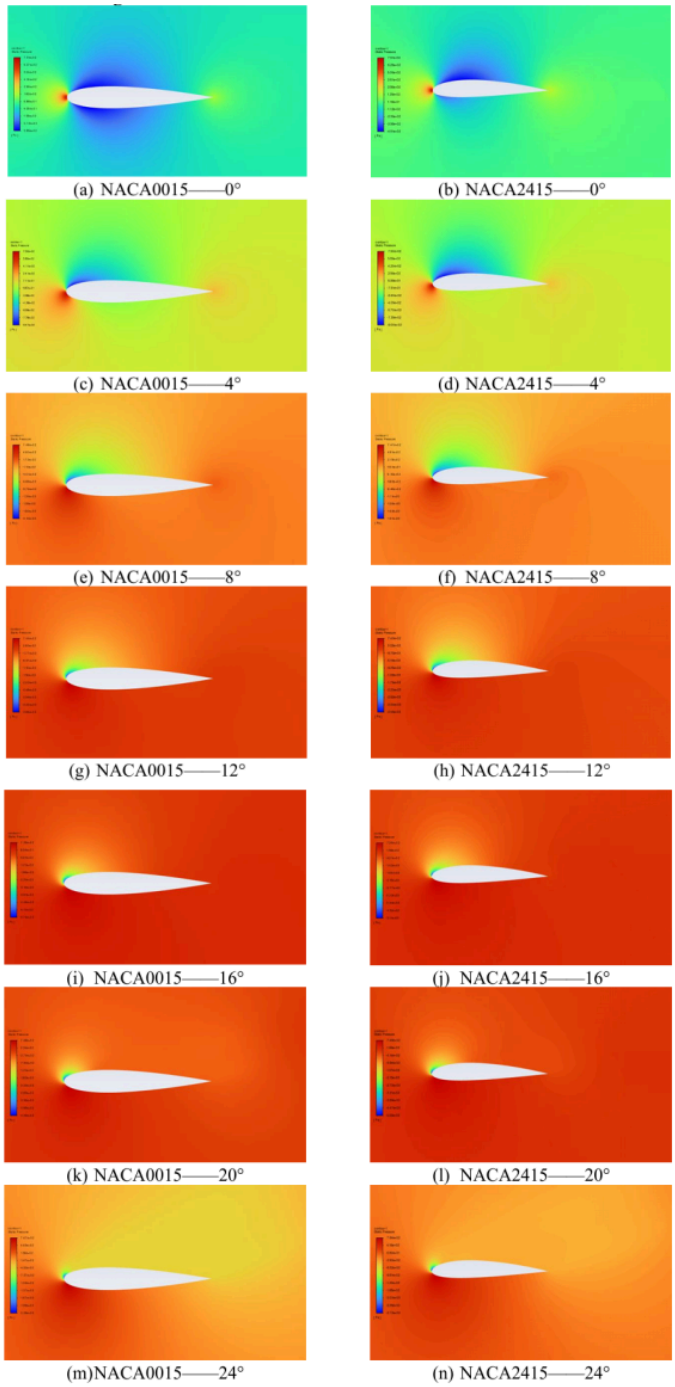

Figure 6. Comparison of pressure contour plots for NACA0015 and NACA2415 at different angles of attack

DOI: 10.54254/2755-2721/2026.38264

As clearly shown in Figure 6, at the same low attack angle, both the coverage area of the low-pressure region on the upper surface of the NACA2415 airfoil and the magnitude of its negative pressure are greater than those of the NACA0015 airfoil; consequently, the pressure difference is larger, and the lift coefficient is higher.

3.4. Lift-drag ratio

As shown in Figure 7, the lift-to-drag performance of the NACA2415 airfoil is overall superior to that of the NACA0015 airfoil within the attached flow regime; both airfoils achieve their optimal aerodynamic efficiency at an attack angle of 8°. When the attack angle exceeds this optimal value, flow separation induces a sharp increase in drag, causing a steep fall of the lift-to-drag ratio;the curved profile configuration effectively enhances the overall aerodynamic efficiency across the entire operating range of the airfoil. Furthermore, at low attack angles, the NACA2415 airfoil exhibits superior overall aerodynamic efficiency.

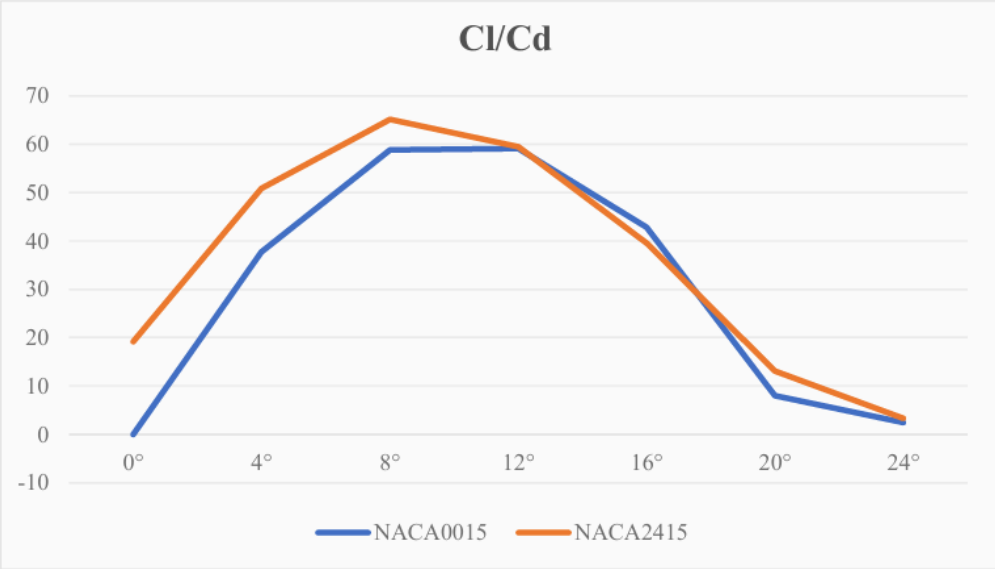

Figure 7. Lift-to-drag ratio of NACA0015 and NACA2415 at various angles of attack

4. Conclusion

This study systematically compares the aerodynamic characteristics of the NACA0015 and NACA2415 airfoils at 0°~24° using CFD numerical simulation, and draws the following conclusions.

(1) The NACA2415 airfoil exhibits a higher lift-to-drag ratio at low speeds and small angles of attack. This indicates that for the same lift, an aircraft equipped with the NACA2415 airfoil suffers lower aerodynamic drag and requires less thrust, thereby reducing energy consumption and extending the endurance when applied to fixed-wing cargo UAVs.

(2) At the cruise angle of attack, the NACA2415 airfoil achieves a larger lift coefficient. With identical wing area, the aircraft can carry a greater payload, making it more suitable for cargo transportation missions.

(3) Under the same Reynolds number in this study, the fluctuation amplitude of the lift coefficient of the NACA2415 airfoil within the stall region is smaller than that of NACA0015, demonstrating superior stall resistance.

DOI: 10.54254/2755-2721/2026.38264

References

[1] Kankanawadi, N., Karinagshetru, G., Patil, L., Ultheru, B., Baruch, J., & Nallusamy, T. (2021). Conceptual design of a fixed wing vertical take-off and landing unmanned aerial vehicle. In *AIP Conference Proceedings (Volume 2341)*(1), 020030. AIP Publishing LLC.

[2] Orvi, T. A., Hossain, I., & Hassan, M. (2025). Computational and experimental investigation of lower-surface dimple effects on NACA 0015 airfoil aerodynamics. *Engineering Science and Technology, an International Journal, 72*, 102228.

[3] Rubel, R. I., Uddin, M. K., Islam, M. Z., & Rokunuzzaman, M. (2016). Comparison of aerodynamics characteristics of NACA 0015 & NACA 4415.

[4] Pane, M. (2023). Wing simulation using NACA 2412 and 2415 airfoils with variations in angle of attack for lift and drag. *VANOS Journal of Mechanical Engineering Education, 8*(2), 190–199.

[5] Zhao, Y., Yang, Y., & Li, M. (2025). The lift on an airfoil at various angles of attack in turbulent flow. *Journal of Fluid Mechanics, 1010*, A45.

[6] Matyushenko, A. A., & Garbaruk, A. V. (2016, November). Adjustment of the k-ω SST turbulence model for prediction of airfoil characteristics near stall. In *Journal of Physics: Conference Series (Vol. 769, No. 1, p. 012082)*. IOP Publishing.

[7] Panagiotou, P., & Yakinthos, K. (2020). Aerodynamic efficiency and performance enhancement of fixed-wing UAVs. *Aerospace Science and Technology, 99*, 105575.

[8] Panagiotopoulos, I., Sakellariou, L., & Hatziefremidis, A. (2024). Design, construction, and flight performance of an electrically operated fixed-wing UAV. *Drones, 8*(6), 217.

[9] Ravikumar, T., & Prakash, D. S. (2014). Aerodynamic analysis of supercritical NACA SC (2)-0714 airfoil using CFD. *Int. J. Adv. Tech. Eng. Sci, 2*(7), 285-293.

[10] Bhaskaran, R., & Collins, L. (2002). Introduction to CFD basics. *Cornell University-Sibley School of mechanical and aerospace engineering*, 1-21. Retrieved from https://dragonfly.tam.cornell.edu/teaching/mae5230-cfd-intro-notes.pdf.